

Modern Physics Letters B  
 © World Scientific Publishing Company

## Spectral Properties of Magnetic Excitations in Cuprate Two-Leg Ladder Systems

Kai P. Schmidt

*Institut für theoretische Physik, Universität zu Köln, Zülpicher Str. 77  
 D-50937 Köln, Germany  
 ks@thp.uni-koeln.de*

Götz S. Uhrig

*Theoretische Physik, Geb. 38, FR 7.1, Universität des Saarlandes  
 D-66123 Saarbrücken, Germany  
 uhrig@lusi.uni-sb.de*

Received (received date)

Revised (revised date)

This article reviews the recent development in the microscopic modeling of the magnetic excitations in cuprate two-leg ladder systems. The microscopic Hamiltonian comprises dominant Heisenberg exchange terms plus an additional four-spin interaction which is about five times smaller. We give an overview over the relevant energies like the one-triplon dispersion, the energies of two-triplon bound states and the positions of multi-triplon continua and over relevant spectral properties like spectral weights and spectral densities in the parameter regime appropriate for cuprate systems. It is concluded that an almost complete understanding of the magnetic excitations in undoped cuprate ladders has been obtained as measured by inelastic neutron scattering, inelastic light (Raman) scattering and infrared absorption.

### 1. Introduction

The origin of high-temperature superconductivity in layered cuprates is still heavily debated. Nevertheless, it has become evident in the last years that the important physics takes place in the two-dimensional copper-oxide planes<sup>1,2</sup>. At zero doping, these compounds are insulating long-range ordered antiferromagnets which are described by (extended) Heisenberg models<sup>3</sup>. On doping, they can be viewed as doped Mott insulators<sup>4</sup>. Doping destroys the antiferromagnetic order rapidly. At some finite value of doping, the superconducting state is realized.

The long-range ordered Néel state at zero doping suggests to base a microscopic description on magnons which interact with the doped holes. But the holes destroy the ordered Néel state giving rise to a spin-liquid state with short range antiferromagnetic correlations. Thus, it would be more appropriate to set up a microscopic description in terms of the elementary excitations of the spin-liquid state, which can be fractional  $S = 1/2$  spinons<sup>5</sup> or integer  $S = 1$  triplons<sup>6</sup>. Their interplay with the doped holes

2 *Kai P. Schmidt and Götz S. Uhrig*

is expected to be crucial for the understanding of the pairing mechanism. But a quantitative theory is so far not in sight.

There is a different class of systems which are spin liquids already in the undoped case due to their lower dimensionality<sup>7,8</sup>, namely the cuprate two-leg ladders. Two-leg ladders have a finite spin gap<sup>9,10,11,12</sup> and the elementary excitations are triplons with  $S = 1$ . The ground states of these ladders can be viewed as realizations of the so-called resonance valence bond (RVB) state, a coherent superposition of singlet dimers, proposed by Anderson for the two-dimensional cuprates<sup>1,13</sup>. Thus, the physical understanding of the cuprate ladders as doped spin liquids is an important step to the understanding of the two-dimensional cuprates.

In this work, our current understanding of the undoped cuprate ladders is reviewed. There has been decisive progress in the understanding of these systems both in theory<sup>14,15,16,17,18,19,20,21</sup> and in experiment<sup>22,23,24,25,26,27</sup>. It is found that a microscopic modeling of the magnetic degrees of freedom has to include a four-spin interaction besides the usual nearest-neighbor Heisenberg exchange. The size of the four-spin exchange in cuprate ladders is determined to be about 20% of the leading nearest-neighbour Heisenberg exchange<sup>19</sup>.

This review is set up as follows. In Sect. 2, we introduce the cuprate ladder compounds, the microscopic model and we give a short overview of the recent developments. Then we present a sketch of the method we use to describe the two-leg ladder system. In the sequel, the major properties of the two-leg ladder system are explored in the parameter regime relevant for the cuprate ladders. In Sect. 4 the spectral weights are discussed. Sect. 5 describes the energy properties, namely the one-triplon dispersion, the energies of the two-triplon bound states and the positions of the multi-triplon continua. The last two parts, Sects. 6 and 7, deal with important spectral densities. The focus is laid on the dynamical structure factor (DSF) which is relevant for inelastic neutron scattering (INS). A short overview of inelastic light scattering, i.e. Raman spectroscopy (RS), and infrared absorption (IR) is given. The review is summarized in Sect. 8

## 2. Cuprate Ladders and the Microscopic Model

### 2.1. Materials

Realizations of two-leg ladders are established in  $\text{SrCu}_2\text{O}_3$  (Sr123)<sup>28,29</sup> and  $\text{A}_{14}\text{Cu}_{24}\text{O}_{41}$  (A14) with  $\text{A}=\{\text{Sr},\text{Ca},\text{La}\}$ <sup>30,31</sup> compounds. The fundamental building block in both compounds are edge-sharing copper-oxide plaquettes where adjacent copper ions are linked linearly to one another by intercalated oxygen ions. (In A14 corner-sharing plaquettes occur also; they give rise to spin chains. But the corresponding energy scale is much lower and we do not focus on them here.)  $\text{Sr}_{0.4}\text{Ca}_{13.6}\text{Cu}_{24}\text{O}_{41}$  becomes superconducting for high pressure<sup>29</sup> enhancing the interest in this class of compounds in particular.

$\text{SrCu}_2\text{O}_3$  is the prototype of a system of weakly coupled  $\text{Cu}_2\text{O}_3$  spin-ladders. The relevant orbitals of the copper atoms are the planar  $d_{x^2-y^2}$  orbitals. The superexchange runs via the  $p_x$  or  $p_y$  orbitals of the intermediate oxygen<sup>32</sup>. The interladder coupling

is significantly smaller because the superexchange via a Cu-O-Cu path with a 90° angle is reduced due to the vanishing overlap of the orbitals<sup>32,33,34</sup>. In addition, the interladder coupling is frustrated because the spin on one ladder is coupled equally to two adjacent spins on the neighboring ladder. The disadvantage of  $\text{SrCu}_2\text{O}_3$  is that it has to be grown under very high pressure so that only small single crystals or polycrystals are available<sup>35</sup>. This hampers the momentum resolution and the counting statistics of scattering experiments, in particular of neutron scattering investigations.

The second class of compounds are the so-called telephone-number compounds  $\text{A}_{14}\text{Cu}_{24}\text{O}_{41}$  with  $\text{A}=\{\text{Sr},\text{Ca},\text{La}\}$ , see left panel in Fig. 1<sup>36</sup>. Two sorts of planes occur. One sort of planes consists of two-leg  $\text{Cu}_2\text{O}_3$  ladders as described in the last paragraph. The other sort consists of corner-sharing  $\text{CuO}_2$  chains. Both one-dimensional structures, ladders and chains, respectively, are oriented along the c-axis. The two sorts of planes are illustrated on the right hand side of Fig. 1. It is instructive to write  $\text{A}_{14}\text{Cu}_{24}\text{O}_{41} = (\text{A}_2\text{Cu}_2\text{O}_3)_7(\text{CuO}_2)_{10}$  in order to emphasize the existence of two structures. This formula assumes a commensurate ratio of seven rungs in the ladders matching ten copper sites in the chains. But closer investigation reveals that this is only an approximation; the ratio is in fact incommensurate, see e.g. Ref. <sup>37</sup> and references therein.

Ladders and chains form two-dimensional layers which are stacked in b-direction in alternation with  $\text{A} \in \{\text{Sr, Ca, La}\}$  layers, see left panel in Fig. 1. Large single crystals of A14 can be grown fairly easily so that inelastic neutron scattering investigations of high resolution are possible.

The distance between two copper atoms is roughly the same in rung and in leg direction. The typical order of magnitude of the nearest-neighbor Heisenberg coupling is 1000 K. It is similar to the one in the two-dimensional cuprates forming square lattices<sup>38,39</sup>. The coupling between two copper atoms on neighboring ladders is weakly ferromagnetic due to the bonding angle of 90°<sup>32,33,34</sup>. The nearest-neighbor exchange coupling in the chains is mediated via two symmetric Cu-O-Cu bonds with about 90° bonding angle implying a weakly ferromagnetic coupling. Its typical value is an order of magnitude smaller than the couplings in the ladders<sup>38</sup>. The difference in energy scales makes it possible to study the behavior of both substructures, ladders and chains, separately.

Two telephone number compounds, namely  $\text{Sr}_{14}\text{Cu}_{24}\text{O}_{41}$  (Sr14) and  $\text{La}_6\text{Ca}_8\text{Cu}_{24}\text{O}_{41}$  (La6Ca8) are the focus of this work. The system Sr14 is intrinsically doped with 6 holes per unit cell. Using X-ray absorption spectroscopy, it is possible to conclude that there are on average 0.8 holes in the ladders and 5.2 holes in the chains<sup>40</sup> which can be explained by a higher electronegativity in the chains<sup>41</sup>.

It is possible to substitute  $\text{Sr}^{2+}$  by isovalent  $\text{Ca}^{2+}$  or by trivalent  $\text{La}^{3+}$  or  $\text{Y}^{3+}$ . The substitution by  $\text{La}^{3+}$  reduces the number of holes in the system. The limiting case of an undoped sample is reached by the (formal) compound La6Ca8. So far, crystal growth has not been able to realize La6Ca8. But there exist crystals up to  $\text{La}_{5.2}\text{Ca}_{8.8}\text{Cu}_{24}\text{O}_{41}$  which can be already be viewed as (almost) undoped sample<sup>24,26</sup>.

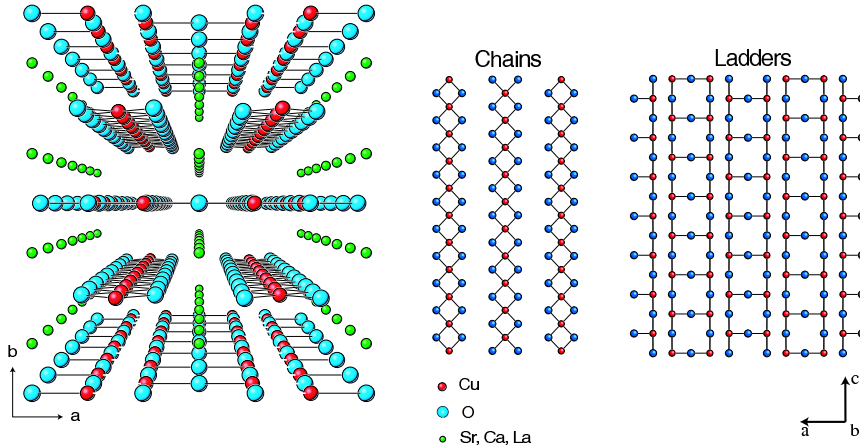


Fig. 1: (color online) Schematic view of the telephone number compound A14. The left panel is a three-dimensional view in the layered material. There are planes of ladder structures (plane at the bottom, in the middle and at the top), of chain structure (the third and the seventh plane) and the planes containing the A cations. The top views of the ladder plane ( $\text{Cu}_2\text{O}_3$ ) and of the chain plane ( $\text{CuO}_2$ ) are shown in the panels on the right side.

## 2.2. Minimal Microscopic Model

Usually only Heisenberg exchange couplings are considered in the description of the magnetic properties of insulating electronic systems. It has been realized early by Dirac<sup>42</sup> and it was later introduced in condensed matter physics by Thouless<sup>43</sup> that the general expression for the exchange Hamiltonian reads

$$H_{\text{ex}} = \sum_{n=2}^{\infty} \sum_{\alpha_n} J_{\alpha_n} (-1)^{P_{\alpha_n}} \Pi_{\alpha_n} \quad , \quad (1)$$

where  $\Pi_{\alpha_n}$  denotes a permutation operator of the localized spins. The sum runs over all permutations labelled by  $\alpha_n$  of  $n$  spins.  $P_{\alpha_n}$  is the parity of the permutation  $\Pi_{\alpha_n}$ . From the physics point of view, these permutations correspond to the exchange of  $n$  spins. The first term represents the well-known two-particle exchange which is usually the dominant contribution.

The importance of the exchange processes with more than two particles was realized first in the description of the magnetism of solid  $^3\text{He}$ <sup>44</sup>. In  $^3\text{He}$ , the two-particle exchange is small due to a hardcore repulsion of the atoms leading to steric blocking. Thus, higher exchange processes, especially the four-spin exchange, are the dominant exchange processes.

The situation in cuprate systems is different than in solid  $^3\text{He}$  because the dominant exchange is the nearest-neighbor Heisenberg exchange. Nevertheless, the derivation of

effective low-energy Heisenberg models from realistic three-band<sup>44,45,46,47,48</sup> and one-band<sup>49,50,51</sup> Hubbard models showed that the four-spin ring exchange is the dominant *correction* to the standard nearest-neighbour Heisenberg exchange. The value of the four-spin ring exchange obtained from these studies is about 20% of the dominant Heisenberg exchange.

To be precise, we denote the Hamiltonian of the two-leg ladder with additional four-spin ring exchange by

$$H^p = \frac{J_\perp^p}{2} \sum_i \Pi_{i,1;i,2} + \frac{J_\parallel^p}{2} \sum_{i,\tau} \Pi_{i,\tau;i+1,\tau} + H_{\text{cyc}}^p \quad (2)$$

$$H_{\text{cyc}}^p = \frac{J_{\text{cyc}}^p}{4} \sum_{\langle i j k l \rangle} \left( \Pi_{i j k l} + \Pi_{i j k l}^{-1} \right) .$$

Here  $\Pi_{i,j}$  is the permutation operator of two-particles,  $i$  labels the rungs and  $\tau \in \{1, 2\}$  the legs, the composite index  $\tilde{i} = (i, \tau)$  combines the rung and the leg information. Then the permutation operator of four spins is  $\Pi_{i j k l}$  where  $\langle i j k l \rangle$  restricts the sum to four spins on a plaquette.

It is convenient to introduce spin operators and to rewrite (2) in terms of a Heisenberg model plus additional four-spin interactions<sup>14</sup>

$$H = J_\perp \sum_i \mathbf{S}_{i,1} \mathbf{S}_{i,2} + J_\parallel \sum_{i,\tau} \mathbf{S}_{i,\tau} \mathbf{S}_{i+1,\tau} + H_{\text{cyc}} \quad (3)$$

$$H_{\text{cyc}} = J_{\text{cyc}} \sum_{\text{plaquettes}} \left[ (\mathbf{S}_{1,i} \mathbf{S}_{1,i+1}) (\mathbf{S}_{2,i} \mathbf{S}_{2,i+1}) + (\mathbf{S}_{1,i} \mathbf{S}_{2,i}) (\mathbf{S}_{1,i+1} \mathbf{S}_{2,i+1}) \right. \\ \left. - (\mathbf{S}_{1,i} \mathbf{S}_{2,i+1}) (\mathbf{S}_{1,i+1} \mathbf{S}_{2,i}) \right] . \quad (4)$$

Both Hamiltonians (Eq. 2 and Eq. 3) are the same up to two-spin interactions along the diagonal of the spin ladder. It is known that these couplings are small (of the order of  $0.03 J_\perp$ <sup>46</sup>) so that we restrict the discussion in the following to the Hamiltonian in Eq. 3. Note that both Hamiltonians are in use in the literature. The relation between the exchange parameters of both Hamiltonians reads

$$J_\perp = J_\perp^p + \frac{1}{2} J_{\text{cyc}}^p \quad (5)$$

$$J_\parallel = J_\parallel^p + \frac{1}{4} J_{\text{cyc}}^p \quad (6)$$

$$J_{\text{cyc}} = J_{\text{cyc}}^p . \quad (7)$$

A first experimental indication for the relevance of the four-spin ring exchange was conjectured on the basis of the line shape of IR data<sup>52</sup> for planar cuprates. An unambiguous experimental signature was found by INS in  $\text{La}_2\text{CuO}_4$  in 2001<sup>39</sup>. The spin-wave dispersion can be explained only by the inclusion of four-spin interactions. The Raman line shape also points towards a significant four-spin exchange coupling<sup>53,54</sup>. Recently, the value of 20% ring exchange coupling was also found in the stripe-ordered phase of  $\text{La}_{1.875}\text{Ba}_{0.125}\text{CuO}_4$ <sup>55</sup>.

First hints towards a four-spin interactions in cuprate ladders was found in 1999 by INS<sup>38,14,56,23</sup> for  $\text{La}_6\text{Ca}_8$ . The fits of the experimentally measured one-triplon

dispersion by the results for the standard Heisenberg model yielded  $J_{\parallel}/J_{\perp} \approx 2$  where  $J_{\parallel}$  is the coupling along the legs and  $J_{\perp}$  the one along the rungs of the ladder. The very large deviation of this ratio from unity appears astounding in view of the geometrical structure of the cuprate ladders which is fairly isotropic. The inclusion of the four-spin ring exchange can resolve this discrepancy. But the INS data is not complete enough to determine the value for the four-spin interaction quantitatively.

A quantitative determination was possible on the basis of IR data combined with INS data on the spin gap. The IR data provides information on bound states<sup>24,19</sup>. Theoretically, the key development was a systematic approach to high-order perturbation theory for multi-particle states and bound states in particular<sup>57,58,59,15,16,17,60,61</sup>. Even spectral densities can be computed in the framework of this recently developed approach which is based on a controlled change of basis, i.e. unitary transformations<sup>16,18,62</sup>.

These developments rendered the systematic and quantitative calculation of two-triplon bound states<sup>11,63,64,65,66,67,15,68,16</sup> possible. A calculation in linear order in  $J_{\parallel}/J_{\perp}$  predicted that a bound state has a large effect on the IR line shape<sup>68</sup>. The quantitative calculation in the regime  $J_{\parallel} \approx J_{\perp}$  revealed that the experimental data for La6Ca8<sup>24</sup> is described by a more isotropic exchange of  $J_{\parallel} \approx 1.3J_{\perp}$ <sup>24</sup>. The Raman line shape also indicated that  $J_{\parallel}/J_{\perp} \approx 1$  is the appropriate range for cuprate ladders<sup>18</sup>.

The first quantitative determination of the three most important exchange constants in cuprate ladders ( $J_{\perp}$ ,  $J_{\parallel}$  and  $J_{\text{cyc}}$ ) was done by density-matrix renormalization analyzing IR data for La6Ca8<sup>19</sup>. The values obtained are  $J_{\parallel}/J_{\perp} \approx 1.2 - 1.3$  and  $J_{\text{cyc}}/J_{\perp} \approx 0.2 - 0.25$ . RS revealed that the cuprate ladder compounds Sr14<sup>25</sup> and Sr123<sup>27</sup> differ slightly from La6Ca8. Recently, it was shown that a unified description of the Raman response for all three compounds is possible<sup>69</sup>. Both Sr14 and Sr123 are described by  $x := J_{\parallel}/J_{\perp} \approx 1.4 - 1.5$  and  $x_{\text{cyc}} := J_{\text{cyc}}/J_{\perp} \approx 0.2 - 0.25$ . The values for Sr14 are consistent those for IR data for this compound<sup>70,71</sup>.

If we allow the parameters  $x$  and  $x_{\text{cyc}}$  to vary freely including sign changes there is a variety of quantum phases which occurs depending on the parameters<sup>72,73,74,75,76,77,21,78,79</sup>. The generic cuprate ladders, however, are in the so-called rung-singlet phase<sup>21,79</sup>. This is the massive phase which is adiabatically connected to the two-leg spin ladder without ring exchange. This system at  $x_{\text{cyc}} = 0$  does not display any phase transition for  $x \in (0, \infty)$ <sup>11,12</sup>. At  $x = \infty$  it corresponds to two isolated spin-chains. The ground state of the system is dominated by rung-singlets whence the name rung-singlet phase. It is characterized by a finite rung-triplon gap.

If for a given  $x_{\text{cyc}} > 0$   $x$  is increased further and further the rung-singlet phase becomes unstable against the formation of dimers along the legs. The dimerization is out-of-phase on the two legs yielding a meander structure. But the realistic values  $x \approx 1$  and  $x_{\text{cyc}} \approx 0.2$  ensure that the cuprate ladders are always in the rung-singlet phase. The spin gap is roughly halved due to the finite value of the cyclic exchange so that the quantum phase transition to the dimerized phase is not too far away.

For experimental relevance, this review explores the properties of the two-leg ladder in the rung-singlet phase.

### 3. Method

In this part, the essential points concerning the continuous *unitary* transformations (CUTs) are discussed<sup>80,81,82,58</sup>. Here we use a particle-conserving perturbative CUT<sup>60,61,83</sup> which uses the states on isolated rungs as reference. The Hamiltonian of a spin ladder plus additional four-spin interaction (Eq. 3) is re-expressed by

$$\frac{H(x)}{J_\perp} = H_\perp + xH_\parallel + x_{\text{cyc}}H_{\text{cyc}} \quad (8)$$

with  $x = J_\parallel/J_\perp$  and  $x_{\text{cyc}} = J_{\text{cyc}}/J_\perp$  as perturbation parameters.

The CUT is defined by

$$\partial_I H(I) = [\eta(I), H(I)] \quad (9)$$

to transform  $H(I=0) = H$  from its initial form (8) to an effective Hamiltonian  $H_{\text{eff}} := H(I=\infty)$  which *conserves* the number elementary triplet excitations on the rungs, the so-called triplons<sup>6</sup>. Formally, the conservation of triplons is expressed by  $0 = [H_\perp, H_{\text{eff}}]$ . An appropriate choice of the infinitesimal generator  $\eta$  is given by the matrix elements

$$\eta_{i,j}(I) = \text{sgn}(q_i - q_j) H_{i,j}(I) \quad (10)$$

in an eigen basis of  $H_\perp$ ; the  $q_i$  are the corresponding eigen values<sup>58</sup>.

The perturbative realization of the CUT provides a series expansion for the various parts of the effective Hamiltonian: the one-triplon hopping amplitudes and the triplon-triplon interaction. We have calculated the hopping amplitudes up to order 11 and the triplon-triplon interaction up to order 10 in  $x$  and  $x_{\text{cyc}}$ .

Next, the observables of interest in the ladder system have to be evaluated in order to determine the spectral properties of the two-leg ladder. The observables  $\mathcal{O}$  are transformed by the same CUT

$$\partial_I \mathcal{O}(I) = [\eta(I), \mathcal{O}(I)] \quad . \quad (11)$$

The four *local* operators considered are

$$\mathcal{O}^I(r) = \mathbf{S}_{1,r} \mathbf{S}_{2,r} = \mathcal{T}_0^I \quad (12)$$

$$\mathcal{O}_I^{II}(r) = \mathbf{S}_{I,r} \mathbf{S}_{I,r+1} \quad (13)$$

$$= \frac{1}{4} (\mathcal{T}_{-2} + \mathcal{T}_0 + \mathcal{T}_2 + \mathcal{T}_{-1}^{II} + \mathcal{T}_1^{II})$$

$$\mathcal{O}^{III}(r) = \mathbf{S}_{1,r}^z - \mathbf{S}_{2,r}^z = \mathcal{T}_{-1}^{III} + \mathcal{T}_1^{III} \quad (14)$$

$$\mathcal{O}^{IV}(r) = \mathbf{S}_{1,r}^z + \mathbf{S}_{2,r}^z = \mathcal{T}_0^{IV} \quad . \quad (15)$$

Here  $\mathcal{T}_n$  are local operators changing the triplon number by  $n$ . The explicit action of these operators is given elsewhere<sup>61</sup>. The index  $I = 1, 2$  in Eq. 13 denotes the leg on which the observable operates. In contrast to the triplon-conserving effective Hamiltonian  $H_{\text{eff}}$ , the effective observables also excite or annihilate triplons. The parts which require that an excitation is present before the observable is applied do not matter at zero temperature. We have calculated those parts of the effective observables which correspond to the creation and annihilation of one and two triplons up to order 10.



Fig. 2: The operator  $\mathcal{P}$  reflects about the depicted axis. A *single* singlet on a rung is odd; a triplet on a rung is even with respect to  $\mathcal{P}$ . The action of  $\mathcal{P}$  on the rung-singlet ground state is defined to be of even parity  $\mathcal{P}|0\rangle = |0\rangle$ , i.e. we assume an even number of rungs. If in the triplon vacuum  $|0\rangle$  one singlet is substituted by a triplon, the resulting state  $|1\rangle$  is odd:  $\mathcal{P}|1\rangle = -|1\rangle$ .

The part creating three triplons is determined up to order 8 and for four-triplon parts up to order 7 in  $x$  and  $x_{\text{cyc}}$ .

As it is common in physics the symmetry properties of the injected triplons play an important role. Here we discuss spin and parity. The first two observables  $\mathcal{O}^I$  and  $\mathcal{O}^{II}$  excite triplons with total spin zero. Thus they are relevant for optical experiments like RS and IR. The latter two observables inject triplons with total spin one. They are important to study the DSF relevant for INS experiments.

The parity which is conserved in this ladder system is defined relative to the reflection  $\mathcal{P}$  about the center-line of the ladder, see Fig. 2. If  $|n\rangle$  denotes a state with  $n$  rungs excited to triplons while all other rungs are in the singlet state one finds  $\mathcal{P}|n\rangle = (-1)^n|n\rangle$ , see also caption of Fig. 2. The state  $|n\rangle$  is a linear combination of many  $n$ -triplon states. So no generality is lost in writing

$$\mathcal{O}_{\text{eff}}|0\rangle = \sum_{n \geq 0} |n\rangle. \quad (16)$$

The parity with respect to  $\mathcal{P}$  of the observables introduced in Eqs. 3 is clear from their definition:  $\mathcal{O}^{III}$  is odd while  $\mathcal{O}^I$  and  $\mathcal{O}^{IV}$  are even. The symmetrized observable  $\mathcal{O}^{II} = (\mathcal{O}_1^{II} + \mathcal{O}_2^{II})/2$  is equally even. The parity is conserved in the CUT so that  $\mathcal{P}$  applied to both sides of Eq. (16) requires

$$\mathcal{O}_{\text{eff}}|0\rangle = \begin{cases} \sum_n |2n\rangle, & \mathcal{O}_{\text{eff}} \text{ even} \\ \sum_n |2n+1\rangle, & \mathcal{O}_{\text{eff}} \text{ odd} \end{cases}. \quad (17)$$

An even (odd) parity of  $\mathcal{O}_{\text{eff}}$  implies that  $\mathcal{O}_{\text{eff}}$  injects an even (odd) number of triplons into the system. The relevance of these symmetries will be discussed in more detail in Sects. 6 and 7 where the experimentally relevant results are presented.

The series for the effective Hamiltonian and for the effective observables have to be extrapolated in order to obtain reliable results describing the regime of cuprate ladders. The extrapolation is performed using the one-triplon spin gap  $\Delta$  as internal parameter<sup>84,77,83</sup>. Usually a standard  $[n, 2]$  dlogPadé extrapolant or a  $[n, 2]$  Padé extrapolant is used for the series expressed in  $\Delta$ .

#### 4. Spectral Weights

The analysis of the spectral weights helps to determine the quality of the description in terms of a small number of triplons. If the weight resides mainly in a small number

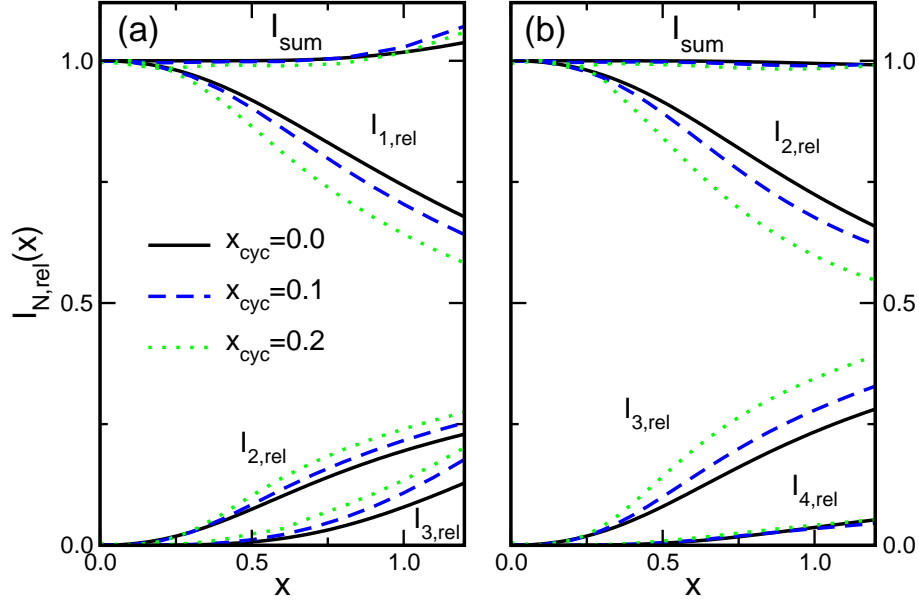


Fig. 3: (color online) (a) Relative weights for the  $S = 1$  operator  $\frac{1}{2}(\mathcal{O}^{\text{III}}(r) + \mathcal{O}^{\text{IV}}(r))$  (Eq. 14 and Eq. 15). The  $I_N$  are calculated up to and including order 10, 10, and 9 in  $x$  for  $N = 1, 2$ , and 3, respectively. The total intensity  $I_{\text{tot}}$  is equal to 1/4. Black solid lines correspond to  $x_{\text{cyc}} = 0$ , dashed (blue) lines to  $x_{\text{cyc}} = 0.1$  and dotted gray (green) lines to  $x_{\text{cyc}} = 0.2$ .  $I_{\text{sum}} = (I_1 + I_2 + I_3)/I_{\text{tot}}$  denotes the sum of all plotted contributions. It is to be compared to unity. (b) Relative weights for the  $S = 0$  operator  $S_{1,i}S_{1,i+1}$  (Eq. 13). The  $I_N$  are calculated up to and including order 10, 8, and 7 in  $x$  for  $N = 2, 3$ , and 4, respectively. The total intensity  $I_{\text{tot}}$  has been extracted from the 11th order result for the ground state energy per spin. Black solid lines correspond to  $x_{\text{cyc}} = 0$ , dashed (blue) lines to  $x_{\text{cyc}} = 0.1$  and dotted gray (green) lines to  $x_{\text{cyc}} = 0.2$ .  $I_{\text{sum}} = (I_2 + I_3 + I_4)/I_{\text{tot}}$  denotes the sum of all plotted contributions.

of channels with a small number of triplons the chosen description works well. If, however, the weight is distributed over a large number of channels the description is less well adapted to the problem. The focus is laid here on the spectral weights for realistic values of the four-spin interaction.

#### 4.1. $S = 1$

First, the spectral weights for excitations with total spin  $S = 1$  are discussed. The local observable considered is the combination of Eq. 14 and Eq. 15

$$\mathcal{O}^{S=1}(r) = \frac{1}{2}(\mathcal{O}^{\text{III}}(r) + \mathcal{O}^{\text{IV}}(r)) . \quad (18)$$

This combination corresponds to the spin operator acting on the spin on leg 1. The spectral weights were calculated up to order 10 in the one- and two-triplon channel, up

to order 9 in the three-triplon channel and up to order 10 in the four-triplon channel. The total spectral weight  $I_{\text{tot}}$  is equal to 1/4 for  $S = 1$  because  $(S^z)^2 = 1/4$ .

In Fig. 3a the relative spectral weights  $I_n/I_{\text{tot}}$  are shown for  $x_{\text{cyc}} = 0$  (black solid lines),  $x_{\text{cyc}} = 0.1$  ((blue) dashed lines) and  $x_{\text{cyc}} = 0.2$  (gray (green) dotted lines) and  $N \in \{1, 2, 3\}$ . In addition, the sum of all plotted relative weights  $I_{\text{sum}} = (I_1 + I_2 + I_3)/I_{\text{tot}}$  is depicted. The sum is very close to unity. Hence contributions with more than three triplons only have negligible weight in the parameter regime displayed.

The general tendency on increasing the four-spin interactions is the reduction of the one-triplon weight and the increase of the weights for two and three triplons. Extrapolating the one-triplon spectral weight by dlogPadé extrapolants, one recognizes poles. This indicates that the one-triplon weight vanishes at the phase transition<sup>77</sup>. The analysis of  $I_2$  in the vicinity of the phase transition indicates that it stays finite at an approximate value of 25%. So it seems that, contrary to the case of the one-dimensional Heisenberg chain<sup>6,85</sup>, the rung-triplon picture breaks down at the phase transition tuned by the four-spin interaction.

The three-triplon sector is extrapolated by a [5, 0] dlogPadé extrapolant because other extrapolants are spoiled by spurious poles. We presume that the depicted extrapolant of the three-triplon weight is affected by the vicinity of such poles so that it overshoots for larger values of  $x$ . This conclusion is supported by the observation that the sum of all plotted relative weights overshoots in the same fashion as the three-triplon weight increases for increasing  $x$ . The extrapolations of the one- and two-triplon sector are very stable so that it is unlikely that they induce the violation of the sum rule for large  $x$ .

Fig. 3a shows that for realistic values of the four-spin interaction the one- and the two-triplon sector contain by far most of the spectral weight. Therefore, the DSF for these two channels provides an almost complete description of INS experiments on cuprate ladders. The corresponding calculation is presented in Sect. 6.

#### 4.2. **S=0**

For the  $S = 0$  case, the local observable  $\mathcal{O}_{\text{eff}}^{\text{II}}$  in Eq. 13 is considered. The total spectral weight  $I_{\text{tot}}(x)$  is calculated reliably from the ground state energy per spin  $\epsilon_0(x)$ <sup>61</sup>.

In Fig. 3b the relative spectral weights  $I_n/I_{\text{tot}}$  are shown for  $x_{\text{cyc}} = 0$  (black solid lines),  $x_{\text{cyc}} = 0.1$  ((blue) dashed lines) and  $x_{\text{cyc}} = 0.2$  (gray (green) dotted lines) and  $N \in \{2, 3, 4\}$ . In addition, the sum  $I_{\text{sum}} = (I_2 + I_3 + I_4)/I_{\text{tot}}$  of all plotted relative weights is depicted. The sum rule is fulfilled quantitatively for all values of  $x_{\text{cyc}}$  depicted in Fig. 3b.

Since a triplon has  $S = 1$  there can be no one-triplon contribution  $I_1$  to the  $S = 0$  response. The  $I_2$  contribution is the leading one. Similar to the  $S = 1$  case, the leading contribution loses spectral weight upon switching on  $x_{\text{cyc}}$ . Simultaneously, triplon sectors with more triplons gain spectral weight. The two-triplon sector contains only about 50% of the spectral weight for realistic parameters ( $x_{\text{cyc}} \approx 0.2, x \gtrsim 1$ ). This means that there are sizable contributions from more triplons. This is seen in optical experiments<sup>86</sup> where three-triplon contributions are important. In addition,

the four-triplon sector matters also, giving rise to finite life times (see below around Fig. 4).

In summary, the analysis of the spectral weights shows that the description where rung triplons are taken as quasi-particles works very well. In the regime of parameters which matters for cuprate ladders, the sectors with low numbers of triplons capture the essential physics. Sectors with more triplons play a certain, but minor, role.

## 5. Energy Properties

The purpose of this section is to illustrate the energetic properties of the two-leg ladder with four-spin interaction in the rung-singlet phase. The influence of the four-spin interactions on the relevant energies is investigated. The focus is laid on the one-triplon dispersion, on the energies of the two-triplon bound states and on the position of the multi-triplon continua. In Figs. 4 and 5 the most relevant energies are shown for  $x = 1$  with  $x_{\text{cyc}} = 0$  and  $x_{\text{cyc}} = 0.2$ . The results found are qualitatively generic for  $x = 1.0 - 1.5$  and  $x_{\text{cyc}} = 0 - 0.25$ .

### 5.1. One-Triplon Dispersion

The one-triplon dispersion can be calculated by several techniques<sup>7,87,14,19,77</sup>. In the left panel of the Figs. 4 and 5 the one-triplon dispersion is shown for  $x = 1$  with  $x_{\text{cyc}} = 0$  and  $x_{\text{cyc}} = 0.2$ . The one-triplon dispersion displays a global minimum at  $k = \pi$  which defines the one-triplon gap  $\Delta$ . Additionally, a local minimum exists at  $k = 0$ . This minimum can be understood as a crossover property to the physics of spin-chains where the dispersion at  $k = 0$  and at  $k = \pi$  are degenerate for the infinite system. It is caused by level repulsion between the one-triplon state and the three-triplon continuum which approaches the one-triplon state more and more as  $x \rightarrow \infty$ . The three-triplon continuum is displayed as gray lines in the left panels of Figs. 4 and 5.

The main effect of the four-spin interaction is a global shift of the one-triplon dispersion to lower energies. The overall shape of the dispersion is almost unchanged. The gap is reduced considerably up to a factor of 2 for  $x_{\text{cyc}} = 0.2$ . This property especially explains the importance of the four-spin interaction for a quantitative description of cuprate ladders.

### 5.2. Two-Triplon Continuum and Bound States

Regarding two-triplon energies not only the one-particle kinetics of the two triplons but also the two-triplon interaction is important<sup>15,16,61</sup>. Generally, one has a two-triplon continuum and two-triplon bound states for a given total momentum. The two-triplon energies are shown as black lines in the right panel of Figs. 4 and 5.

There are two regimes. For small momenta  $k < 0.35\pi$ , bound states are absent and a wide two-triplon continuum is present. For larger momenta  $k > 0.35\pi$  and  $x_{\text{cyc}} = 0$ , there are two bound states below the two-triplon continuum. There is one bound state with total spin  $S = 1$  and one with total spin  $S = 0$ . The binding energy

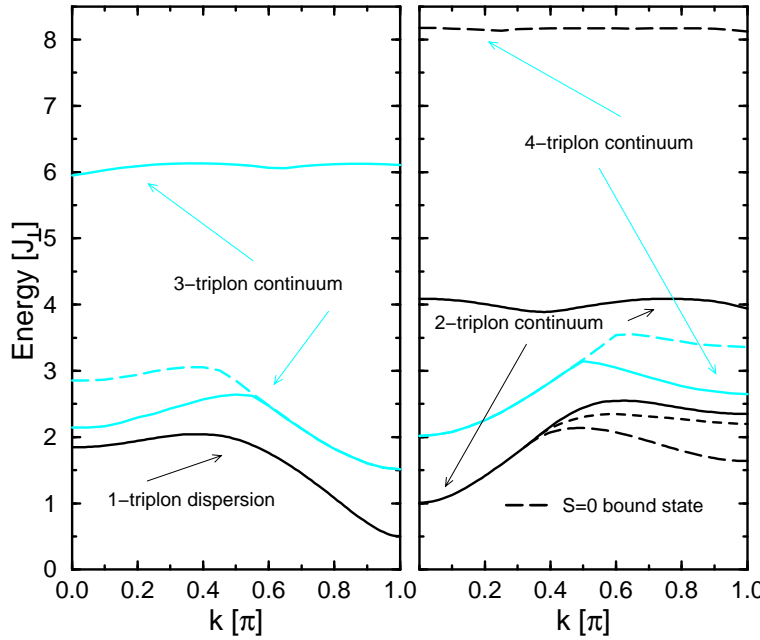


Fig. 4: (color online) Multi-triplon continua of the two-leg ladder for  $x = 1$  and  $x_{\text{cyc}} = 0$ . One- and three-triplon energies are shown in the left panel while two- and four-triplon energies are depicted in the right panel, since the sectors of even and of odd number of triplons do not couple. Left panel: the solid black line denotes the one-triplon dispersion  $\omega(k)$ . The gray (cyan) solid lines correspond to the lower and to the upper band edge of the three-triplon continuum including two-triplon binding effects. The dashed gray (cyan) lines denote the lower band edge of the three-triplon continuum neglecting two-triplon binding. Right panel: the solid black lines correspond to the lower and to the upper edge of the two-triplon continuum. The dashed black line corresponds to the two-triplon bound states. The solid gray (cyan) lines denote the lower and the upper band edge of the four-triplon continuum including two-triplon binding effects. The dashed gray (cyan) line depicts the lower band edge of the four-triplon continuum neglecting two-triplon binding.

of the  $S = 0$  bound state is by a factor 2 to 4 larger than the binding energy of the  $S = 1$  bound state which is as expected in an antiferromagnet. The dispersion of both bound states has a maximum at  $k \approx 0.5\pi$  and a minimum at  $k = \pi$ .

Since a finite four-spin exchange shifts the one-triplon dispersion to lower energies, also the two-triplon energies are shifted globally to lower energies. The shape of the

lower and the upper edge of the two-triplon continuum remains almost unchanged by the four-spin exchange because the band edges solely determined by the one-triplon dispersion.

The effect of the four-spin interaction on the binding energy of the two-triplon bound states (black dashed lines in Fig. 4 and Fig. 5) is most interesting. The four-spin interaction reduces the attractive interaction between the triplons. Thus the binding energy of the bound states is reduced upon increasing  $x_{\text{cyc}}$ <sup>19</sup>. This effect is present for total spin  $S = 0$  and for total spin  $S = 1$ . The effect is more pronounced in the  $S = 1$  case because the  $S = 1$  two-triplon bound state is less tightly bound. As a consequence, the  $S = 1$  bound state is absent for  $x_{\text{cyc}} = 0.2$ . The disappearance of the  $S = 1$  bound state has interesting effects on the spectral line shape of the two-triplon contribution to the dynamical structure factor which will be discussed in Sect. 6.

### 5.3. Multi-Triplon Continua

Next the relative positions of the multi-triplon continua are investigated. The determination of the multi-triplon band edges in combination with the multi-triplon spectral weights (see Sect. 4) is important to estimate possible life-time effects which are neglected in the extrapolation procedure. Recall that the generator (10) orders the states according to their number of triplons. This works perfectly if the energy of a state with  $n+2$  triplons has a higher energy than all states with  $n$  or less triplons<sup>58,88</sup>. But this is not always case, see e.g. Figs. 4 and 5. If the correlation between triplon number and energy is not valid the state with less triplons can decay into the state with more triplons. This hybridization implies an additional broadening of the spectral densities. It can be viewed as a finite life-time effect. In this regime, the perturbative CUT based on the generator (10) works only approximately. The life-time effects are neglected.

For simplicity, the  $n$ -triplon interactions with  $n > 2$ <sup>60</sup> are not included in the calculation of the band edges. They are expected to be very small<sup>89</sup>.

The reduction of the one-triplon gap  $\Delta$  by the four-spin interaction brings all multi-triplon continua closer together in energy. The lower band edge of the three-triplon continuum is very close to the one-triplon dispersion for  $k \in [0, 0.4\pi]$  (left panels). The value for the edge of the three-triplon continuum at  $k = 0$  is the sum of the one-triplon gap and the  $S = 0$  two-triplon bound state energy at  $k = \pi$ .

The situation for two and four triplons is depicted in the right panels of Figs. 4 and 5. Both continua overlap strongly for both parameter sets. The overlap of the two- and four-triplon continuum is larger in the  $S = 0$  case than in the  $S = 1$  case due to the larger binding energy of the  $S = 0$  two-triplon bound state. Therefore, life-time effects are expected to be smaller in the  $S = 1$  case. Moreover, the total spectral weight in the four-triplon channel with  $S = 1$  is very small. Possible effects of the neglected processes are discussed later in the sections dealing with spectral densities and with the interpretation of optical experiments.

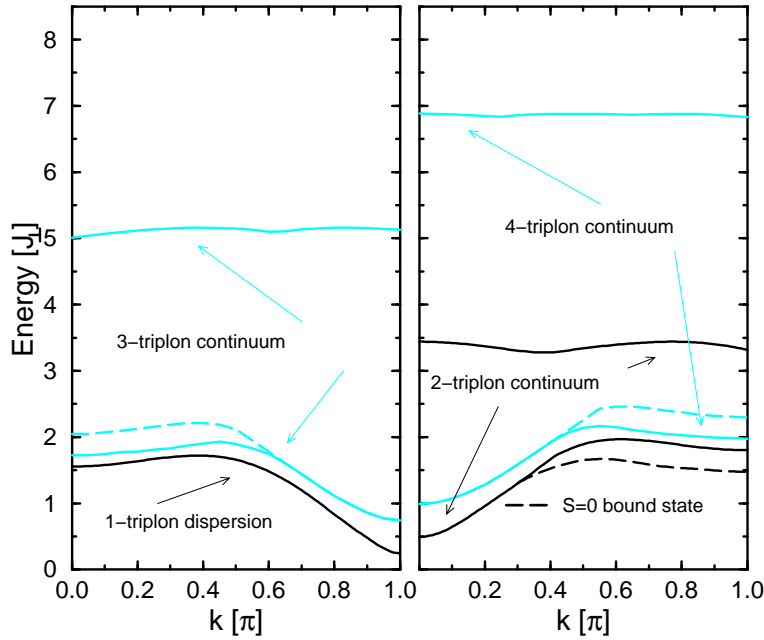


Fig. 5: (color online) Multi-triplon continua of the two-leg ladder for  $x = 1$  and  $x_{\text{cyc}} = 0.2$ . One- and three-triplon energies are depicted in the left panel while two- and four-triplon energies are depicted in the right panel. The notations are the same as in Fig. 4.

## 6. Dynamical Structure Factor (DSF)

This part deals with the DSF of the two-leg spin ladder with four-spin interaction. Results for the one- and the two-triplon contribution which capture most of the spectral weight (see Sect. 4) are shown. The obtained spectral densities are directly relevant for INS experiments.

In the discussion of the parity as defined in Sect. 3, we found that the observable  $\mathcal{O}^{\text{III}}$  has an odd parity while the observable  $\mathcal{O}^{\text{IV}}$  has an even parity. Thus, the observable  $\mathcal{O}^{\text{III}}$  excites only an odd number of triplons and the observable  $\mathcal{O}^{\text{IV}}$  excites even number of triplons. It follows that the by far most important one- and two-triplon contributions can be measured *independently* by INS because the two contributions have a different parity. In particular, the two-triplon contribution should be accessible by the experiment because it is the leading contribution with an even parity.

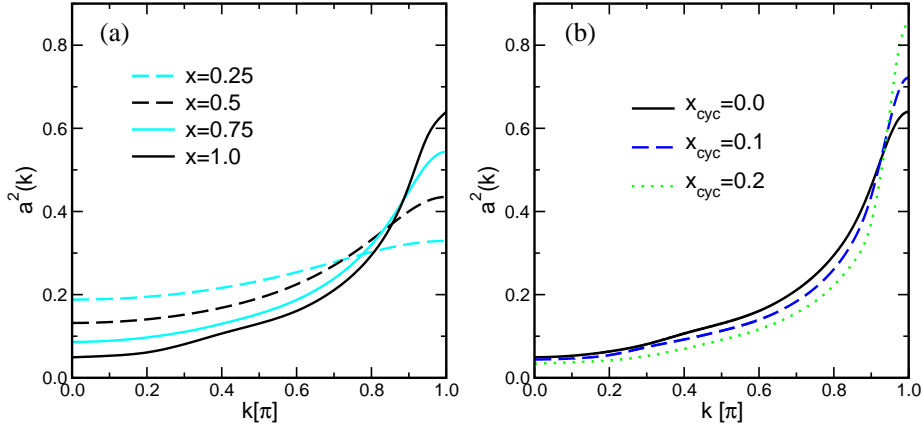


Fig. 6: (color online) The one-triplon spectral density  $l_1(k)$  for  $\mathcal{O}^{III}$  is shown for (a)  $x_{cyc} = 0$  and various values of  $x = \{0.25; 0.5; 0.75; 1.0\}$  and for (b)  $x = 1$  and various values of  $x_{cyc} = \{0; 0.1; 0.2\}$ .

### 6.1. One-Triplon Contribution

The most important contribution to the dynamical structure factor is the one-triplon contribution. The spectral weight accumulates around  $k = \pi$ . Upon increasing  $x$ , the spectral weight decreases for small momenta and concentrates more and more at  $k = \pi$  as illustrated in Fig. 6a.

The effect of the four-spin interaction on the one-triplon spectral weight is exemplified in Fig. 6b for  $x = 1$  with  $x_{cyc} = 0$  (solid black line),  $x_{cyc} = 0.1$  (dashed (blue) line) and  $x_{cyc} = 0.2$  (dotted gray (green) line). It can be seen clearly in Fig. 6b that the effect of  $x_{cyc}$  on the  $k$ -resolved one-triplon spectral weight is similar to the effect of  $x$ . The spectral weight is reduced at small momenta but it increases around  $k = \pi$ . These findings suggest that the one-triplon spectral weight close the phase transition to the out-of-phase dimerization is governed by the physics at  $k = \pi$ . Similar results were also found by exact diagonalisation<sup>90</sup>.

### 6.2. Two-Triplon Contribution

The two-triplon contribution to the dynamical structure factor is the leading part with even parity. Its total spectral weight increases slightly by turning on  $x_{cyc}$  (see Sect. 4). The generic relative spectral weight is about 20% to 30% of the leading one-triplon contribution for realistic values of cuprate ladders.

In Fig. 7 the result for the two-triplon contribution to the dynamical structure factor is shown for  $x = 1$  and  $x_{cyc} = 0$  (a),  $x_{cyc} = 0.1$  (b) and  $x_{cyc} = 0.2$  (c). As discussed in Sect. 5.2 the four-spin interaction has a strong influence on the  $S = 1$  two-triplon bound state. The attractive interaction is lowered by the four-spin interaction which induces interesting changes in the line shape of the two-triplon

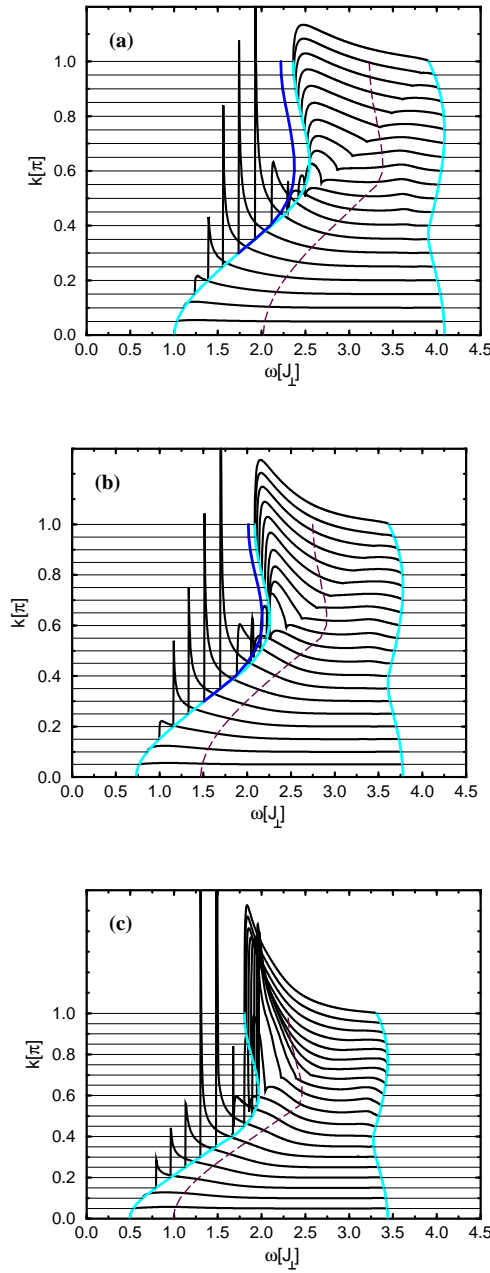


Fig. 7: (color online) The two-triplon spectral density  $l_2(k, \omega)$  for  $\mathcal{O}^{\text{IV}}$  with  $x = 1.0$  and  $x_{\text{cyc}} = 0.0$  (a),  $x_{\text{cyc}} = 0.1$  (b) and  $x_{\text{cyc}} = 0.2$  (c). The gray (cyan) lines denote the lower and the upper edge of the two-triplon continuum. The black lines indicate the dispersion of the  $S = 1$  two-triplon bound state. The long-dashed dark lines depict the lower edge of the  $S = 1$  four-triplon continuum.

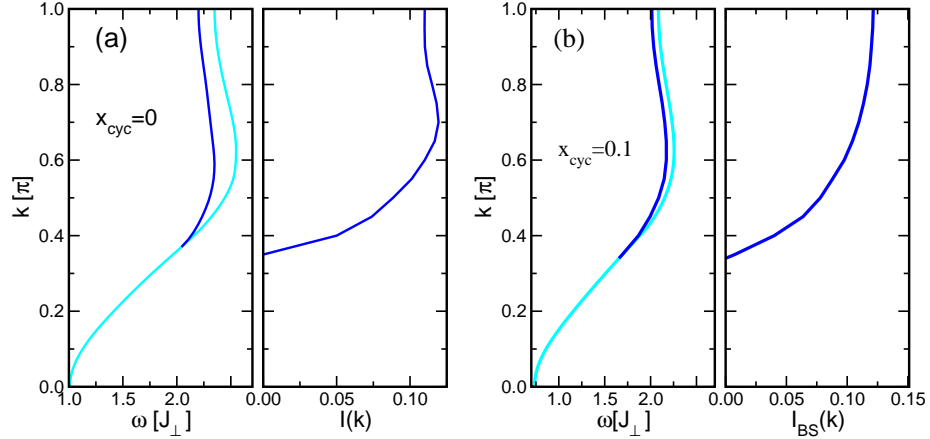


Fig. 8: (color online) The  $S = 1$  two-triplon bound state energy and the spectral weight for  $x = 1.0$  with (a)  $x_{\text{cyc}} = 0$  and with (b)  $x_{\text{cyc}} = 0.1$ . Left panels: The solid gray (cyan) line denotes the lower edge of the two-triplon continuum and the solid black line depicts the dispersion of the  $S = 1$  two-triplon bound state. Right panels: The momentum-resolved spectral weight of the  $S = 1$  two-triplon bound state is shown.

spectral density.

The dispersion of the  $S = 1$  two-triplon bound state is denoted as a solid black line in Fig. 7 and in the left panels of Fig. 8. In the right panels of the latter figure the  $k$ -resolved spectral weight of the bound state is depicted. On increasing  $x_{\text{cyc}}$ , the binding energy and the spectral weight of the bound state is reduced. At  $x_{\text{cyc}} = 0.2$ , the  $S = 1$  two-triplon bound state has disappeared because the overall attractive interaction has become too small.

The reduction of the binding energy of the two-triplon bound state results in a sharpening of the spectral density at the lower band edge. The effect is most prominent near  $k = \pi$ . At the value of  $x_{\text{cyc}}$  where the bound state is degenerate with the lower edge of the two-triplon continuum, the spectral density displays an inverse square root divergence. This corresponds closely to our findings for the dimerized and frustrated spin-chain at certain values of the exchange couplings<sup>85</sup>. At  $x_{\text{cyc}} = 0.2$ , where the two-triplon bound state has already dissolved in the two-triplon continuum, the very sharp structures near the lower band edge are the remaining signature of this divergence.

The lower band edge of the  $S = 1$  four-triplon continuum is depicted by long dashed lines in Fig. 7. It can be seen that the overlap of the two-triplon and the four-triplon continuum increases with increasing four-spin interaction. Nevertheless, possible life-time effects are expected to be of minor importance because most of the two-triplon spectral weight is located below the lower band edge of the four-triplon continuum. In addition, the spectral weight of the four-triplon continuum increases only very slowly like  $l_4(\omega) \propto (\Delta\omega)^{13/2}$  at the lower band edge<sup>89</sup> where  $\Delta\omega$  measures

the distance to the band edge. This extremely slow increase results from the hard-core repulsion of the triplons which makes them behave like fermions at low energies because the system is one-dimensional.

## 7. Optical Experiments

In this section, two-triplon spectral densities with total spin  $S = 0$  are analyzed. The effect of the four-spin interaction on the energy spectrum was already discussed in Sect. 5.2. In contrast to the  $S = 1$  case studied in the last section, the  $S = 0$  two-triplon bound state is present also for finite  $x_{\text{cyc}}$  in the range of parameters considered here. Thus, the impact of the four-spin interaction on the line shape of the two-triplon spectral density is less pronounced than in the  $S = 1$  case.

In the sequel, the complete two-triplon contribution is discussed first focusing on  $x = 1$ . The general trends are the same for other values of  $x$ . The second and the third part deal with the two-triplon contribution to RS and IR. In all parts, results are presented for the observable  $\mathcal{O}^I$  acting on the rungs and for the observable  $\mathcal{O}^{II}$  acting on the legs of the spin ladder.

### 7.1. Two-Triplon Contribution

The two-triplon contribution comprises most of the spectral weight in the  $S = 0$  sector (see Sect. 4). Nevertheless, the three- and four-triplon spectral weights are sizable for  $x \geq 1$  and especially for finite  $x_{\text{cyc}}$ . The latter contributions have to be kept in mind when comparing the results to experimental data and in estimating possible neglected life-time effects. Recall that the observable  $\mathcal{O}^I$  has only contributions with an even number of triplons while the observable  $\mathcal{O}^{II}$  includes contributions of odd and even number of triplons.

In Fig. 9 results for  $x = 1$  with  $x_{\text{cyc}} = 0.0$  (a) and  $x_{\text{cyc}} = 0.2$  (b) are shown. The upper panels depict the findings for  $\mathcal{O}^I$  and the lower panels depict the results obtained for  $\mathcal{O}^{II}$ . Detailed information about the  $S = 0$  two-triplon bound state dispersion and its  $k$ -resolved spectral weight is presented in Fig. 10.

The first effect to note is that the overall line shape of the two-triplon spectral density hardly changes in the  $S = 0$  case when the four-spin interaction is switched on. As in the  $S = 1$  sector, there is a global shift to lower energies at finite  $x_{\text{cyc}}$  resulting from the change of the one-triplon dispersion.

Both observables yield the same line shape for  $k = 0$  and  $x_{\text{cyc}} = 0$ <sup>91,18</sup>. This symmetry holds only at  $k = 0$ ; it is broken for finite  $x_{\text{cyc}}$ . Nevertheless, even at  $x_{\text{cyc}} = 0.2$  the line shape for both observables is very similar for small momenta. A more detailed discussion of the  $k = 0$  contribution will be given in the next subsection about RS. For large momenta, however, the responses for the two observables differ.

The next important effect of the four-spin interaction besides the global shift to lower energies is the decrease of the binding energy near  $k = \pi$ . The loss of binding energy can be seen clearly in Fig. 10. This effect is accompanied by a reduction of spectral weight of the bound state near  $k = \pi$ , see right panels of Fig. 10. The spectral weight is transferred to the two-triplon continuum which becomes sharper on

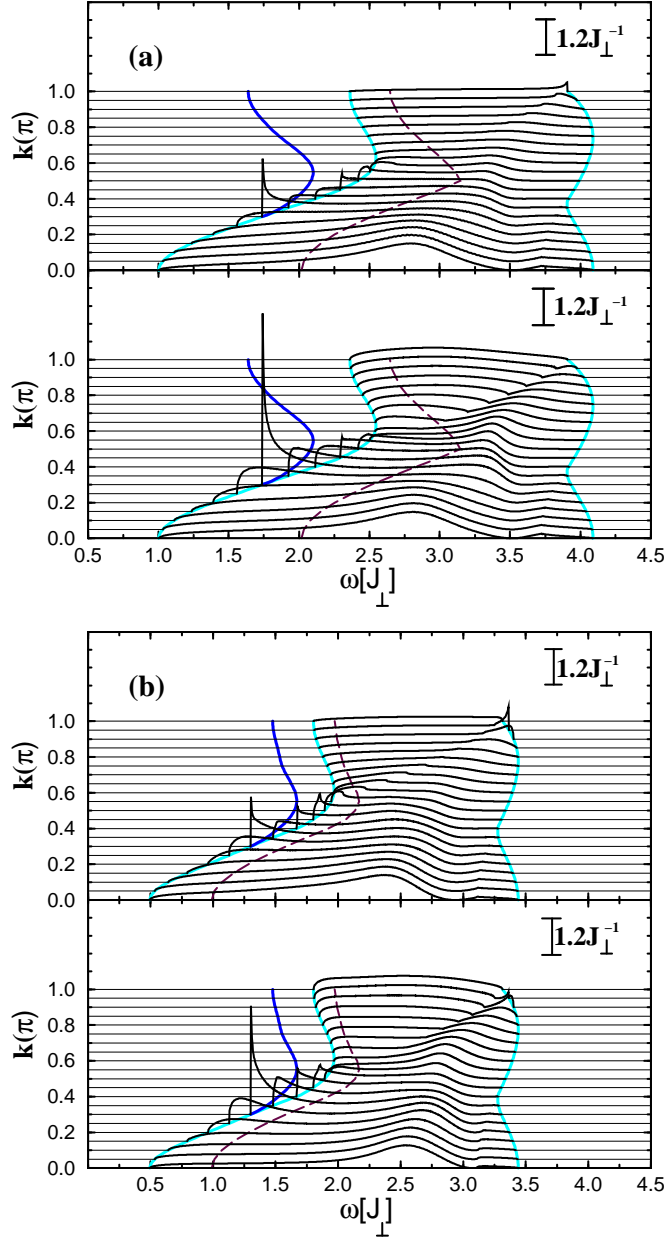


Fig. 9: (color online) Two-triplon spectral density  $l_2(k, \omega)$  with  $S = 0$  at  $x = 1.0$  with  $x_{\text{cyc}} = 0.0$  (a) and with  $x_{\text{cyc}} = 0.2$  (b). The upper panels correspond to  $\mathcal{O}^I$  and the lower panels to  $\mathcal{O}^{II}$ . The gray (cyan) lines denote the lower and the upper edge of the two-triplon continuum. The black (blue) lines indicate the dispersion of the  $S = 0$  two-triplon bound state. Long-dashed lines depict the lower edge of the  $S = 1$  four-triplon continuum.

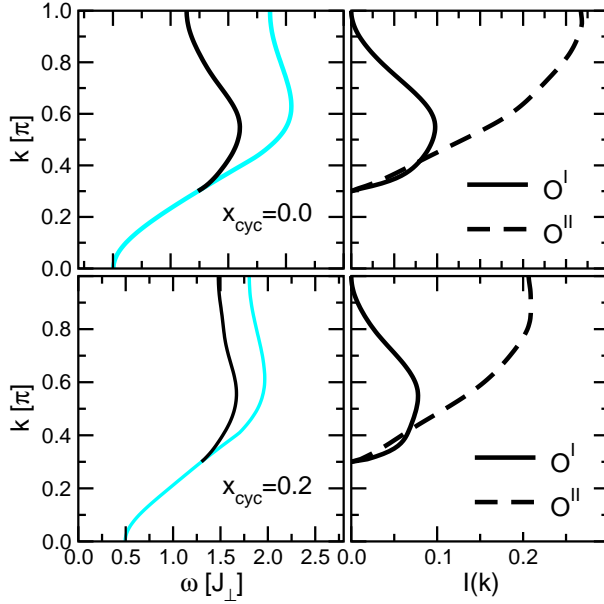


Fig. 10: (color online) Energy and spectral weight of the two-triplon  $S = 0$  bound states for  $x = 1.0$  with  $x_{\text{cyc}} = 0.0$  (upper panel) and  $x = 1.0$  with  $x_{\text{cyc}} = 0.2$  (lower panel). Left panels: The solid gray (cyan) line denotes the lower edge of the two-triplon continuum and the solid black line depicts the dispersion of the  $S = 0$  two-triplon bound state. Right panels: The momentum-resolved spectral weight of the  $S = 0$  two-triplon bound state is plotted as measured by  $\mathcal{O}^I$  (solid line) and by  $\mathcal{O}^{II}$  (dashed line).

increasing  $x_{\text{cyc}}$ .

The black long-dashed curve in Fig. 9 represents the lower band edge of the  $S = 0$  four-triplon continuum. The overlap of the two- and four-triplon continuum is larger in the  $S = 0$  case than in the  $S = 1$  case due to the larger binding energy of the  $S = 0$  two-triplon bound state. The overlap is slightly enhanced by the four-spin interactions. Note that the two-triplon bound state is located below the four-triplon continuum for all momenta so that no finite life-time effects are neglected for this part of the two-triplon contribution.

Furthermore, the two-triplon contribution displays only broad features for large momenta and energies above the long dashed curve. Therefore life-time effects will have only minor effects on this part of the spectrum because a small additional broadening will not change much. This is different for small momenta where relatively sharp structures are present which will be affected by including possible decays of two triplon states into four triplon states.

## 7.2. Raman Spectroscopy

This subsection deals with the two-triplon contribution to the non-resonant Raman response. The observables for magnetic light scattering in rung-rung (leg-leg) polarization are the  $k = 0$  part of  $\mathcal{O}^I$  ( $\mathcal{O}^{II}$ )<sup>92,93,91,18,20,69</sup>. Here only a short summary of the most important results is given. The reader who is interested in further details is referred to more specialized papers<sup>18,20,69</sup>.

Channels with an odd number of triplons are inaccessible by Raman scattering due to the invariance of the observables with respect to reflection about the centerline of the ladder, see discussion on the parity in Sect. 3. Thus only excitations with an even number of triplons matter. The relevant contributions to the Raman response come from the 2-triplon and the 4-triplon sector. The two-triplon contribution is the most important one, cf. Sect. 4.

The line shape does not depend on the observable for  $x_{\text{cyc}} = 0$  because the Hamiltonian is a weighted sum of the two of them  $H = \mathcal{O}^I(k = 0) + x\mathcal{O}^{II}(k = 0)$  up to a global factor<sup>91,18</sup>. Thus the excited state  $\mathcal{O}^I(k = 0)|0\rangle$  equals  $-x\mathcal{O}^{II}(k = 0)|0\rangle$  except for a component proportional to the ground state  $|0\rangle$  which does not represent an excitation. The Raman response for  $x_{\text{cyc}} = 0$  is discussed in detail elsewhere<sup>18,69</sup>. The line shape of  $\mathcal{O}^I(k = 0)$  and  $\mathcal{O}^{II}(k = 0)$  for finite  $x_{\text{cyc}}$  is no longer the same. We find that the line shape of  $\mathcal{O}^I(k = 0)$  is almost unchanged by switching on  $x_{\text{cyc}}$ . In contrast, the line shape of  $\mathcal{O}^{II}(k = 0)$  does change. Nevertheless, the overall difference between the line shapes in both polarizations remains small for the realistic parameters discussed in this work. The next important effect of the four-spin interaction besides the global shift to lower frequencies is a sharpening of the dominant two-triplon peak measured by  $\mathcal{O}^{II}(k = 0)$ , i.e., in leg-leg polarization. In addition, an almost constant plateau is produced for frequencies smaller than the two-triplon peak in this polarization.

## 7.3. IR-absorption

In this section a short discussion of phonon-assisted IR of magnetic excitations is presented. The leading infrared-active magnetic absorption is a two-triplon-plus-phonon process<sup>94,95,24</sup>. Note that three- and four-triplon processes contribute also to the IR signal, depending on the exchange couplings of the ladder, see Fig. 3b. As in the previous subsection, we concentrate here on the most important and generic features and we refer to other publications for more detailed discussions<sup>24,19,86</sup>.

The two-triplon spectral density  $I_2(k, \omega)$  has to be integrated over all momenta weighted by a phonon-specific form factor  $|f_{\text{ph}}(k)|^2$ . This yields the two-triplon part of the IR  $I_{2\text{trp}}^{\text{IR}}$ . The precise form of the phonon form factor  $|f_{\text{ph}}(k)|^2$  depends on the specific phonon involved<sup>96</sup>. Different phonons have different form factors so that the sum of several contributions has to be considered. But usually all phonon form factors are largest for large momenta at the zone boundary.

In leg polarization, three features are present in the experimental signals: two peaks at lower energy and a broad hump at higher energies. At lower energy, the line shape is dominated by the two-triplon  $S = 0$  bound state as predicted for small values of

$x^{68}$ . For  $x \gtrsim 0.5$ , the dispersion of the bound state displays a maximum at  $k \approx \pi/2$  and a minimum at  $k = \pi$ , see Sect. 5.2. Both give rise to van Hove singularities in the density of states which cause the peaks in  $I_{2\text{trp}}^{\text{LR}}$ <sup>24</sup>. The spectral weight of the bound state has a maximum at  $k = \pi$  for  $\mathcal{O}^{\text{II}}$ , see Fig. 10. Thus the two-triplon contribution in leg polarization shows two peaks originating from the extrema of the dispersion of the two-triplon bound state. The intensity of the energetically lower peak is larger. The peaks are more clearly seen for larger values of  $x$  because the difference between maximum and minimum of the two-triplon bound state dispersion increases with increasing  $x$ . The third feature, the broad hump, originates from the two-triplon continuum and from three-triplon contributions<sup>19,89</sup>.

In rung polarization, the three features are also present but the intensity is distributed differently. The spectral weight of the two-triplon bound state vanishes at  $k = \pi$  (Fig. 10). Thus the energetically lowest van Hove singularity appears only as low-energy shoulder. It becomes more pronounced for larger  $x$  values. The dominant peak results from the van Hove singularity at  $k \approx \pi/2$  where the spectral weight is finite. The broad hump induced by the two-triplon continuum is more important in this polarization because the two singularities at lower energies carry less weight.

In leg polarization, channels with both odd and even number of triplons contribute. The analysis of the spectral weights, see Sect. 4, has shown that the three-triplon channel contributes significantly. This was to be expected from earlier DMRG calculations<sup>19</sup>. Due to the reflection symmetry of the observable, contributions with odd parity are absent in rung polarization. Therefore, the next important correction is only the four-triplon contribution which carries little weight, see Sect. 4. Moreover, its line shape can be expected to be rather featureless and broad, because as many as four particles are involved so that momentum conservation does not have a very important impact.

## 8. Summary and Conclusion

In this article the spectral properties of magnetic excitations in cuprate two-leg ladder systems have been reviewed. A quantitative microscopic description comprises two-spin and four-spin interactions. The undoped cuprate ladders are always in the rung-singlet phase, i.e. there is an adiabatic connection to the state of isolated rung dimers. The elementary excitation is a triplon. The exchange couplings generically take the values  $x = J_{\parallel}/J_{\perp} = 1.2 - 1.5$ ,  $x_{\text{cyc}}/J_{\perp} \approx 0.2$  and  $J_{\perp} = 1000 - 1200\text{cm}^{-1}$ .

The accuracy of the description in terms of rung triplons in the regime relevant for the cuprate ladders was discussed by means of the spectral weights. It has been found that the leading one- and two-triplon channels contain the dominant weight. A sizable three-triplon contribution is found for total spin  $S = 0$ . The one- and two-triplon channels dominate the physics for realistic values of the coupling constants for cuprate ladders.

Various energies are important: the one-triplon dispersion, the energies of bound states consisting of two triplons and the positions of the multi-triplon. The main effect of the four-spin interaction is a global red shift to lower energies. As a consequence, the continua approach each other. The two- and the four-triplon continua especially

overlap more strongly. The second sizable effect of the four-spin interaction is to lower the attractive two-triplon interaction. Thereby the binding energy of the two-triplon bound states is reduced and spectral weight is shifted from the bound state to the two-triplon continuum. The  $S = 1$  bound state has disappeared for realistic values of cuprate ladders due to this effect.

The dynamical structure factor is dominated by the one-triplon contribution. Most of the spectral weight is found at the zone boundaries where the spin gap occurs. The spectral weight for small momenta is very low. The two-triplon contribution represents about 30% of the total spectral weight integrated over all momenta, frequencies and parities. The two-triplon contribution is the leading one with even parity. Thus it should be measurable independently from the one-triplon contributions. The shape of the two-triplon continuum for total spin  $S = 1$  changes significantly for finite four-spin interaction. The disappearance of the two-triplon bound state causes sharp structures at the lower band edge of the two-triplon continuum.

The spectral densities with total spin  $S = 0$  are relevant for RS and IR. The electromagnetic waves couple to the rungs or the legs of the ladder leading to a pronounced dependence on the polarization. The RS measures the response at zero total momentum. There the spectrum is dominated by the two-triplon peak within the two-triplon continuum. The IR displays a structure with three peaks. The two low-energy features originate from the two-triplon bound state. The third very broad peak represents the continuum contribution. The overall shape of the  $S = 0$  spectral density is not changed significantly for realistic values of the four-spin interaction.

The interplay of recent developments in the theoretical description of gapped one-dimensional spin liquids and the improvements in spectroscopic experiments have permitted to gain a quantitative understanding of the magnetic excitations and their line shapes in cuprate ladder systems.

Fruitful discussions are acknowledged with M. Grüninger, A. Gößling, A. Läuchli, A. Reischl, S. Dusuel, S. Trebst, H. Monien, D. Khomskii, and E. Müller-Hartmann. This work was supported by the DFG in SFB 608 and in SP 1073.

## References

1. P. W. Anderson, *Science* **235**, 1196 (1987).
2. P. W. Anderson, *The Theory of Superconductivity in the High- $T_c$  Cuprate Superconductors* (Princeton University Press, New Jersey, 1997).
3. E. Manousakis, *Rev. Mod. Phys.* **63**, 1 (1991).
4. J. Orenstein and A. J. Millis, *Science* **288**, 468 (2000).
5. L. D. Faddeev and L. A. Takhtajan, *Phys. Lett.* **85A**, 375 (1981).
6. K. P. Schmidt and G. S. Uhrig, *Phys. Rev. Lett.* **90**, 227204 (2003).
7. T. Barnes, E. Dagotto, J. Riera, and E. S. Swanson, *Phys. Rev. B* **47**, 3196 (1993).
8. E. Dagotto and T. M. Rice, *Science* **271**, 618 (1996).
9. E. Dagotto and A. Moreo, *Phys. Rev. B* **38**, 5087 (1988).
10. E. Dagotto, J. Riera, and D. Scalapino, *Phys. Rev. B* **45**, 5744 (1992).
11. D. G. Shelton, A. A. Nersesyan, and A. M. Tsvelik, *Phys. Rev. B* **53**, 8521 (1996).
12. M. Greven, R. J. Birgeneau, and U.-J. Wiese, *Phys. Rev. Lett.* **77**, 1865 (1996).
13. S. Liang, B. Douçot, and P. W. Anderson, *Phys. Rev. Lett.* **61**, 365 (1988).

24 *Kai P. Schmidt and Götz S. Uhrig*

14. S. Brehmer, H. Mikeska, M. Müller, N. Nagaosa, and S. Uchida, *Phys. Rev. B* **60**, 329 (1999).
15. S. Trebst, H. Monien, C. J. Hamer, Z. Weihong, and R. Singh, *Phys. Rev. Lett.* **85**, 4373 (2000).
16. C. Knetter, K. P. Schmidt, M. Grüninger, and G. S. Uhrig, *Phys. Rev. Lett.* **87**, 167204 (2001).
17. W. Zheng, C. J. Hamer, R. R. P. Singh, S. Trebst, and H. Monien, *Phys. Rev. B* **63**, 144410 (2001).
18. K. P. Schmidt, C. Knetter, and G. S. Uhrig, *Europhys. Lett.* **56**, 877 (2001).
19. T. Nunner, P. Brune, T. Kopp, M. Windt, and M. Grüninger, *Phys. Rev. B* **66**, 180404 (2002).
20. K. P. Schmidt, C. Knetter, M. Grüninger, and G. S. Uhrig, *Phys. Rev. Lett.* **90**, 167201 (2003).
21. A. Läuchli, G. Schmid, and M. Troyer, *Phys. Rev. B* **67**, 100409(R) (2003).
22. S. Sugai and M. Suzuki, *phys. stat. sol. (b)* **215**, 653 (1999).
23. M. Matsuda, K. Katsumata, R. S. Eccleston, S. Brehmer, and H.-J. Mikeska, *Phys. Rev. B* **62**, 8903 (2000).
24. M. Windt, M. Grüninger, T. Nunner, C. Knetter, K. P. Schmidt, G. S. Uhrig, T. Kopp, A. Freimuth, U. Ammerahl, B. Büchner, et al., *Phys. Rev. Lett.* **87**, 127002 (2001).
25. A. Gozar, G. Blumberg, B. S. Dennis, B. S. Shastry, N. Motoyama, H. Eisaki, and S. Uchida, *Phys. Rev. Lett.* **87**, 197202 (2001).
26. M. Grüninger, M. Windt, T. Nunner, C. Knetter, K. P. Schmidt, G. S. Uhrig, T. Kopp, A. Freimuth, U. Ammerahl, B. Büchner, et al., *J. Phys. Chem. Solids* **63**, 2167 (2002).
27. A. Gößling, U. Kuhlmann, C. T. A. Löffert, C. Gross, and W. Assmus, *Phys. Rev. B* **67**, 052403 (2003).
28. Z. Hiroi, M. Azuma, M. Takano, and Y. Bando, *J. Solid State Chem.* **95**, 230 (1991).
29. M. Uehara, T. Nagata, J. Akimitsu, H. Takahashi, N. Môri, and K. Kinoshita, *J. Phys. Soc. Jpn.* **65**, 2764 (1996).
30. E. M. McCarron, M. A. Subramanian, J. C. Calabrese, and R. L. Harlow, *Mat. Res. Bull.* **23**, 1355 (1988).
31. T. Siegrist, L. F. Schneemeyer, S. A. Sunshine, and J. V. Waszcak, *Mat. Res. Bull.* **23**, 1429 (1988).
32. P. W. Anderson, *Phys. Rev.* **79**, 350 (1950).
33. J. Goodenough, *Phys. Rev.* **100**, 564 (1955).
34. J. Kanamori, *J. Phys. Chem. Solids* **10**, 87 (1959).
35. A. Löffert, C. Gross, and W. Assmus, *J. Crystal Growth* **237-239**, 796 (2002).
36. U. Ammerahl (PhD Thesis, Universität zu Köln, 2000).
37. S. van Smaalen, *Z. Kristallogr.* **214**, 786 (1999).
38. R. S. Eccleston, M. Uehara, J. Akimitsu, H. Eisaki, N. Motoyama, and S. Uchida, *Phys. Rev. Lett.* **81**, 1702 (1998).
39. R. Coldea, S. M. Hayden, G. Aeppli, T. G. Perring, C. D. Frost, T. E. Mason, S. W. Cheong, and Z. Fisk, *Phys. Rev. Lett.* **86**, 5377 (2001).
40. N. Nücker, M. Merz, C. A. Kuntscher, S. Gerhold, S. Schuppler, R. Neudert, M. S. Golden, J. Fink, D. Schild, S. Stadler, et al., *Phys. Rev. B* **62**, 14384 (2000).
41. Y. Mizuno, T. Tohyama, and S. Maekawa, *J. Phys. Soc. Jpn.* **66**, 937 (1997).
42. P. A. M. Dirac, *Proc. Roy. Soc. A* **123**, 714 (1929).
43. D. J. Thouless, *Proc. Phys. Soc. Lond.* **86**, 893 (1965).
44. M. Roger and J. M. Delrieu, *Phys. Rev. B* **39**, 2299 (1989).
45. H. J. Schmidt and Y. Kuramoto, *Physica* **B163**, 443 (1990).
46. Y. Mizuno, T. Tohyama, and S. Maekawa, *J. Low Temp. Phys.* **117**, 389 (1999).

47. E. Müller-Hartmann and A. Reischl, *Eur. Phys. J. B* **28**, 173 (2002).
48. C. Calzado, C. de Graaf, E. Bordas, R. Caballol, and J.-P. Malrieu, *Phys. Rev. B* **67**, 132409 (2003).
49. M. Takahashi, *J. Phys. C* **10**, 1289 (1977).
50. A. H. MacDonald, S. M. Girvin, and D. Yoshioka, *Phys. Rev. B* **37**, 9753 (1988).
51. A. Reischl, E. Müller-Hartmann, and G. S. Uhrig, *Phys. Rev. B* **70**, 245124 (2004).
52. J. Lorenzana, J. Eroles, and S. Sorella, *Phys. Rev. Lett.* **83**, 5122 (1999).
53. A. A. Katanin and A. P. Kampf, *Phys. Rev. B* **66**, 100403 (2002).
54. A. A. Katanin and A. P. Kampf, *Phys. Rev. B* **67**, 100404 (2003).
55. G. S. Uhrig, K. P. Schmidt, and M. Grüninger, *Phys. Rev. Lett.* **93**, 267003 (2004).
56. M. Matsuda, K. Katsumata, R. S. Eccleston, S. Brehmer, and H.-J. Mikeska, *J. Appl. Phys.* **87**, 6271 (2000).
57. G. S. Uhrig and B. Normand, *Phys. Rev. B* **58**, R14705 (1998).
58. C. Knetter and G. S. Uhrig, *Eur. Phys. J. B* **13**, 209 (2000).
59. C. Knetter, A. Bühler, E. Müller-Hartmann, and G. S. Uhrig, *Phys. Rev. Lett.* **85**, 3958 (2000).
60. C. Knetter, K. P. Schmidt, and G. S. Uhrig, *J. Phys. A: Math. Gen.* **36**, 7889 (2003).
61. C. Knetter, K. P. Schmidt, and G. S. Uhrig, *Eur. Phys. J. B* **36**, 525 (2004).
62. W. Zheng, C. J. Hamer, and R. R. P. Singh, *Phys. Rev. Lett.* **91**, 037206 (2003).
63. G. S. Uhrig and H. J. Schulz, *Phys. Rev. B* **54**, 9624(R) (1996).
64. G. S. Uhrig and H. J. Schulz, *Phys. Rev. B* **58**, 2900 (1998).
65. K. Damle and S. Sachdev, *Phys. Rev. B* **57**, 8307 (1998).
66. O. P. Sushkov and V. N. Kotov, *Phys. Rev. Lett.* **81**, 1941 (1998).
67. V. N. Kotov, O. P. Sushkov, and R. Eder, *Phys. Rev. B* **59**, 6266 (1999).
68. C. Jurecka and W. Brenig, *Phys. Rev. B* **61**, 14307 (2000).
69. K. P. Schmidt, A. Gössling, U. Kuhlmann, C. Thomsen, A. Löffert, C. Gross, and W. Assmus, *Phys. Rev. B* in press (2005).
70. M. Windt, XXX (PhD Thesis, Universität zu Köln, 2003).
71. M. Grüninger, *private communication* (2005).
72. A. A. Nersesyan and A. M. Tsvelik, *Phys. Rev. Lett.* **78**, 3939 (1997).
73. Y. Honda and T. Horiguchi, condmat/0106426 (2001).
74. K. Hijii and K. Nomura, *Phys. Rev. B* **65**, 104413 (2002).
75. M. Müller, T. Vekua, and H.-J. Mikeska, *Phys. Rev. B* **66**, 134423 (2002).
76. T. Hikihara, T. Momoi, and X. Hu, prl **90**, 087204 (2002).
77. K. P. Schmidt, H. Monien, and G. S. Uhrig, *Phys. Rev. B* **67**, 184413 (2003).
78. T. Momoi, T. Hikihara, M. Nakamura, and X. Hu, *Phys. Rev. B* **67**, 174410 (2003).
79. V. Gritsev, B. Normand, and D. Baeriswyl, *Phys. Rev.* **69**, 094431 (2003).
80. F. J. Wegner, *Ann. Physik* **3**, 77 (1994).
81. S. D. Glazek and K. G. Wilson, *Phys. Rev. D* **48**, 5863 (1993).
82. S. D. Glazek and K. G. Wilson, *Phys. Rev. D* **49**, 4214 (1994).
83. K. P. Schmidt, *Spectral Properties of Quasi One-dimensional Quantum Antiferromagnets Perturbative Continuous Unitary Transformations* (PhD Thesis, available at [www.uni-saarland.de/fak7/uhrig/dissertationen.html](http://www.uni-saarland.de/fak7/uhrig/dissertationen.html), Universität zu Köln, 2004).
84. K. P. Schmidt, C. Knetter, and G. S. Uhrig, *Acta Physica Polonica B* **34**, 1481 (2003).
85. K. P. Schmidt, C. Knetter, and G. S. Uhrig, *Phys. Rev. B* **69**, 104417 (2004).
86. M. Grüninger, M. Windt, E. Benckiser, T. S. Nunner, K. P. Schmidt, G. S. Uhrig, and T. Kopp, in *Advances in Solid State Physics*, edited by B. Kramer (Springer Verlag, Heidelberg, 2003), vol. 43, p. 95.
87. J. Oitmaa, R. R. P. Singh, and Z. Weihong, *Phys. Rev. B* **54**, 1009 (1996).
88. A. Mielke, *Eur. Phys. J. B* **5**, 605 (1998).

89. S. Kirschner, *Multi-Particle Spectral Densities* (Diploma Thesis, available at [www.unisaarland.de/fak7/uhrig/diploma.html](http://www.unisaarland.de/fak7/uhrig/diploma.html), Universität zu Köln, 2004).
90. N. Haga and S. Suga, Phys. Rev. B **66**, 132415 (2002).
91. P. J. Freitas and R. R. P. Singh, Phys. Rev. B **62**, 14113 (2000).
92. P. A. Fleury and R. Loudon, Phys. Rev. **166**, 514 (1968).
93. B. S. Shastry and B. I. Shraiman, Phys. Rev. Lett. **65**, 1068 (1990).
94. J. Lorenzana and G. A. Sawatzky, Phys. Rev. Lett. **74**, 1867 (1995).
95. J. Lorenzana and G. A. Sawatzky, Phys. Rev. B **52**, 9576 (1995).
96. T. Nunner, P. Brune, T. Kopp, M. Windt, and M. Grüninger, Acta Physica Polonica B **34**, 1545 (2003).